The Journal of Neuroscience, May 1994, 14(5): 2503–2514

Developmental Regulation of Voltage-gated K^+ Channel and $GABA_A$ Receptor Expression in Bergmann Glial Cells

T. Müller,[1] J. M. Fritschy,[2] J. Grosche,[1] G. D. Pratt,[2] H. Möhler,[2] and H. Kettenmann[1,3]

[1]Department of Neurobiology, University of Heidelberg, 6900 Heidelberg, Germany, [2]Institute of Pharmacology, University of Zürich, 8057 Zürich, Switzerland, and [3]Max-Delbrück-Center for Molecular Medicine, 13122 Berlin-Buch, Berlin

Bergmann glial cells are closely associated with neurons: during development they provide guiding structures for migrating granule cells and in the adult cerebellum they display intimate interactions with Purkinje cells. In this study, we have addressed the question of whether such changes in neuronal–glial interactions during development are accompanied by variations in the membrane properties of Bergmann glial cells. We used a mouse cerebellum slice preparation to study membrane currents of the Bergmann glial cells at various stages of development *in situ* using the patch-clamp technique. The distinct morphology of Bergmann glial cells was revealed by Lucifer yellow injections during recording. While Bergmann glial cells in mice of postnatal day 20 (P20) to P30 have thick processes with arborized, irregularly shaped leaf-like appendages, the processes of cells from younger mice (P5–P7) are thinner and smoother. This morphological maturation is accompanied by a variation in voltage-gated currents. In cells from P5 to P7, delayed outward- and inward-rectifying K^+ currents were recorded, while older Bergmann glial cells were characterized by, large, voltage- and time-independent K^+ currents. In addition, application of GABA induces two effects, a rapid activation of a Cl^- conductance and a longer-lasting decrease in the (resting) K^+ conductance. Both effects were mediated by benzodiazepine-insensitive $GABA_A$ receptors. Responses in cells of P5–P7 mice were large as compared to the small or even undetectable responses in P20–P30 cells. These $GABA_A$ receptors were characterized immunohistochemically in mice and rat brain sections with five subunit-specific antibodies. Bergmann glial cells exhibit a distinct but transient immunoreactivity for the $GABA_A$ receptor α2-, α3-, and δ-subunits. Staining is maximal between P7 and P10 and decreases gradually thereafter. In contrast, antibodies to the α1- and β2,3-subunits fail to decorate Bergmann glial cells, although they yield a prominent staining of both the Purkinje cells and the granule cells. These changes in the Bergmann glial cell membrane properties and $GABA_A$ receptor expression suggest a transition between functional states during development of the Bergmann glial cells.

[Key words: K^+ channels, $GABA_A$ receptor, patch clamp, cerebellum, thin slices, subunit-specific antibodies, glial cells]

In the developing cerebellum, the Bergmann glial cells play a crucial role as a guiding path for granule cells during their migration from the external granule cell layer to their final destination in the internal granule cell layer. In the mouse, this migratory period lasts at least until postnatal day 20 (P20) and involves a close interaction between granule cells and Bergmann glial cells (Rakic, 1981; Hatten et al., 1990). By contrast, in the mature cerebellum, Bergmann glial cells form an intimate interrelationship with Purkinje cells (Ito, 1984). The functional importance of this neuronal–glial interaction is unknown. To understand further the role of the Bergmann glial cells in these cellular interactions and their possible role in CNS information processing, more information is needed on putative signal transduction mechanisms in these cells, for example, via neurotransmitter receptors and ion channels. In this study, we have addressed the question of whether the change in the neuronal partner of Bergmann glial cells during development is underlined by changes in their membrane properties.

We have shown previously that Bergmann glial cells in slices from mature cerebellum lack voltage-gated K^+, Na^+, and Ca^{2+} channels and are characterized by a large voltage- and time-independent K^+ conductance. In addition, they express a distinct type of kainate receptor (Müller et al., 1992). Activation of these kainate receptors leads to the opening of a channel permeable for Ca^{2+}, as demonstrated with a combined patch-clamp technique and fura-2 imaging approach. The influx of Ca^{2+} ions results in a transient blockade of the large resting K^+ conductance, thus altering the electrical properties of the Bergmann glial cells (Müller et al., 1992).

Among the ionotropic transmitter receptors, $GABA_A$ receptors have also been demonstrated in glial cells in culture and in brain slices (for review, see von Blankenfeld and Kettenmann, 1992). Astrocytic $GABA_A$ receptors differ from neuronal receptors in their allosteric modulation by benzodiazepine receptor ligands: while benzodiazepine agonists increase GABA responses in astrocytes and in neurons, inverse agonists also increase GABA responses in astrocytes, in contrast to their action in neurons (Backus et al., 1988; Bormann and Kettenmann, 1988).

In the present study, we have used the patch-clamp method to characterize membrane currents of Bergmann glial cells during development and to examine the effects of GABA on these currents. Cells were recorded from acute slices of mouse cere-

Received Nov. 17, 1992; revised Aug. 30, 1993; accepted Sept. 14, 1993.

This research was supported by Bundesministerium für Forschung und Technologie, Hermann und Lilly Schilling-Stiftung, Boehringer-Ingelheim-Fonds (Stipendium to T.M.), Swiss National Science Foundation (FNS 31-25688), and Deutsche Forschungsgemeinschaft (SFB 317). We thank T. Berger for excellent technical assistance.

Correspondence should be addressed to Dr. H. Kettenmann, Neurobiologie der Universität Heidelberg, Im Neuenheimer Feld, 345, 69120 Heidelberg, Germany.

bellum of different postnatal ages and their morphology was revealed by infusion of the fluorescent dye Lucifer yellow during recording. These experiments demonstrate that Bergmann glial cells from P5–P12 mice exhibit prominent responses to GABA, mediated by $GABA_A$ receptors insensitive to benzodiazepines. Cells from P20–P30 mice exhibit only small responses. To determine whether these alterations in GABA responsiveness may be attributed to developmental changes in $GABA_A$ receptor expression, the presence of several $GABA_A$ receptor subunits was assessed immunohistochemically in Bergmann glial cells between P1 and P20. Antibodies that recognize five distinct subunits of the $GABA_A$ receptor ($\alpha1$, $\alpha2$, $\alpha3$, $\beta2,3$, and δ) were used. Expression of $GABA_A$ receptor subunit immunoreactivity by Bergmann glial cells was further characterized by double-immunofluorescence staining with antibodies to glial fibrillary acidic protein (GFAP). The results of these morphological studies support the electrophysiological findings, by demonstrating a transient expression of the $\alpha2$-, $\alpha3$-, and δ-subunit immunoreactivity in Bergmann glial cells at P7 and P10, but not at P20. Thus, transient expression $GABA_A$ receptors in Bergmann glial cells may modulate specific neuron–glia interactions early during cerebellar development.

Materials and Methods

Preparation of brain slices and electrophysiological setup. Young mice (postnatal ages P5–P7, P10–P12, and P20–P30) were killed by decapitation and 120 μm slices were cut from the cerebellum. Slices were placed on a coverslip under a nylon mesh in a recording chamber (Edwards et al., 1989) and remained viable for more than 3 hr under these conditions. The chamber was continuously perfused with a salt solution to which drugs could be added. Cell somata and processes of the Bergmann glial cells were visible in water-immersion optics or by infrared video microscopy (Dodt and Zieglgänsberger, 1990; Hamamatsu, Hamamatsu City, Japan). In contrast to the method of Edwards et al. (1989), a separate pipette was not used to blow off cellular debris at the surface of the slice, but a positive pressure was applied through the pipette while it was lowered to the desired position. Membrane currents were measured with the patch-clamp technique in the whole-cell recording configuration (Hamill et al., 1981). Current signals were amplified with conventional electronics (EPC-7 amplifier, List Electronics, Darmstadt, Germany), filtered at 3 kHz, and sampled at 5 kHz by an interface connected to an IBM AT-compatible computer system, which also served as a stimulus generator.

Solutions and electrodes. The standard bathing solution contained (in mM) NaCl, 150; KCl, 5.4; $CaCl_2$, 2; $MgCl_2$, 1; HEPES, 5; and glucose, 10. The pH was adjusted with NaOH to 7.4, and the solution was gassed with O_2. In some experiments an equimolar amount of NaCl was replaced by 5 mM $BaCl_2$, 10 mM 4-aminopyridine (4-AP), or 50 mM tetraethylammonium (TEA). Recording pipettes were fabricated from borosilicate capillaries (Hilgenberg, Malsfeld, Germany) coated with Sigmacote (Sigma), with resistances ranging from 3 to 7 MΩ. The pipettes contained (in mM) KCl, 130; $CaCl_2$, 0.5; EGTA, 5; $MgCl_2$, 2; HEPES, 10; and ATP, 3. The pH was adjusted with NaOH to 7.4. In addition, 1 mg/ml Lucifer yellow was added to this solution. Gilbecamide and pinacidil have been kindly supplied by Merck, Darmstadt, Germany.

Intracellular staining. During recording cells were dialyzed with the patch pipette solution containing Lucifer yellow. To avoid destruction of the cell as the pipette was pulled off after recording, the seal was destroyed by a large hyperpolarizing current injection. Following recording, slices were fixed for 3–5 hr at room temperature in 4% paraformaldehyde and 0.25% glutaraldehyde in 0.1 M phosphate buffer, pH 7.4. Lucifer yellow–filled cells were examined with a microscope equipped with the appropriate filter combination (400–440 nm band pass, 460 nm mirror, 470 nm long pass).

Immunohistochemical staining. The distribution of the $GABA_A$ receptor subunits $\alpha1$, $\alpha2$, $\alpha3$, $\beta2,3$, and δ was analyzed in the cerebellum of mice and rats between P1 (day of birth) and P20. Polyclonal antibodies selective for the subunits $\alpha1$, $\alpha2$, $\alpha3$, and δ were used (Benke et al., 1991a,b,d), as well as the monoclonal antibody bd-17 (Haring et al., 1985), which recognizes both the $\beta2$- and $\beta3$-subunits (Ewert et al., 1990). The animals were anesthetized with chloral hydrate (400 mg/kg) and perfused through the ascending aorta as described by Fritschy et al. (1992). Brains were removed, postfixed for 12–24 hr, and immersed in 10% dimethyl sulfoxide in phosphate-buffered saline (PBS) for cryoprotection. Parasagittal sections (40 μm) cut from frozen blocks with a sliding microtome were incubated overnight in primary antibodies diluted in PBS with 2% normal serum and 0.2% Triton X-100. Sections were then washed with PBS and processed for immunoperoxidase staining (Hsu et al., 1981), using Vectastain Elite kits (Vector Laboratories) and diaminobenzidine hydrochloride as chromogen. Sections were mounted onto gelatin-coated slides, air dried, dehydrated, and coverslipped out of xylene.

Double-immunofluorescence staining experiments with antibodies to GFAP and to the $GABA_A$-receptor $\alpha2$-, $\alpha3$-, and δ-subunits were performed to provide direct evidence for the presence of these subunits in Bergmann glial cells. Sections were incubated overnight in a mixture of primary antibodies raised in different species, washed with PBS, and transferred in PBS containing secondary antibodies coupled to dichlorotriazinylaminofluorescein and Cy3 (Jackson Immunoresearch) (see Fritschy et al., 1992). Colocalization patterns were analyzed by confocal laser microscopy (Bio-Rad, MRC600).

Antibodies against the $\alpha1$-, $\alpha2$-, $\alpha3$-, and δ-subunits of the $GABA_A$ receptors have been characterized previously (Benke et al., 1991a,b,d; Marksitzer et al., 1993). These antibodies were raised in rabbits ($\alpha1$- and δ-subunits) and guinea pigs ($\alpha2$- and $\alpha3$-subunits) against synthetic peptides derived from the cDNA sequences of the respective subunits and coupled to keyhole limpet hemocyanin (see Benke et al., 1991c). Specificity of the immunoreaction was verified by preincubation of the antibodies with their respective antigen peptides (1–10 μg/ml) and by replacing the primary antibodies with nonimmune serum. The staining was abolished in either case.

Results

Morphology of Bergmann glial cells in acute slices

Cerebellar slices from animals of three age groups, P5–P7, P10–P12, and P20–P30, were studied. The Bergmann glial cells were recognized by the location of their somata in the Purkinje cell layer and the smaller size of these somata (7–10 μm diameter) in comparison to the cell bodies of the Purkinje cells. They typically had two or more processes extending radially toward the pial surface, where they formed end-feet. In slices from P5–P7 mice, the external granule layer was prominently visible and the processes of Bergmann glial cells were often covered by differentiating granule cells (Fig. 1). In slices from P10–P12 mice the external germinal layer was much thinner, as the majority of granule cells had migrated to the internal granule cell layer. At P20–P30, the external granule layer was no longer present and the Bergmann glial cell processes were confined to the molecular layer.

Following establishment of the whole-cell recording mode, Bergmann glial cells were filled with Lucifer yellow to visualize their structure after the recording session. Eighty percent of the Bergmann glial cells at P20 were dye coupled, in contrast to cells from younger animals (P6–P10), where no spread of dye to adjacent cells was observed. Figure 2 illustrates the location and shape of two Bergmann glial cells in slices of a P6 and a P20 mouse, respectively. There were three major differences between these two age groups. First, processes of Bergmann glial cells from P20–P30 slices had a mossy appearance caused by "a multitude of lamellae and granular, moderately branching appendages" (Ramon y Cajal, 1896). P5–P7 Bergmann glial cells appeared much smoother due to a lack of these small lateral appendages. Second, young cells extended only few end-feet to the pia (less than six), while Bergmann glial cells from P20–P30 slices formed a dense layer of end-feet originating from more than six processes. Third, many cells from P5–P7 slices, but not

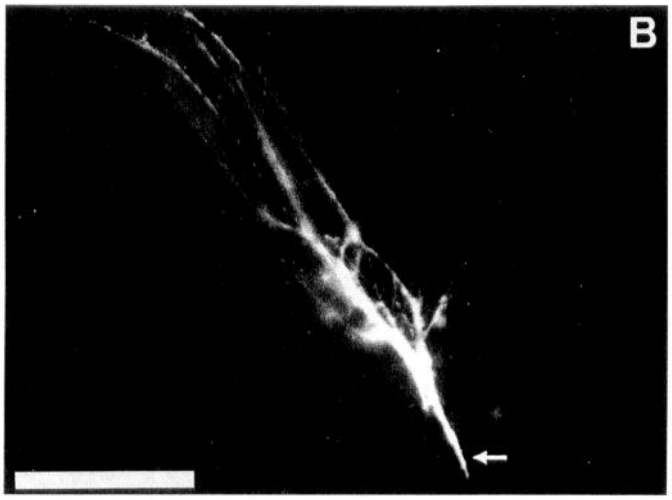

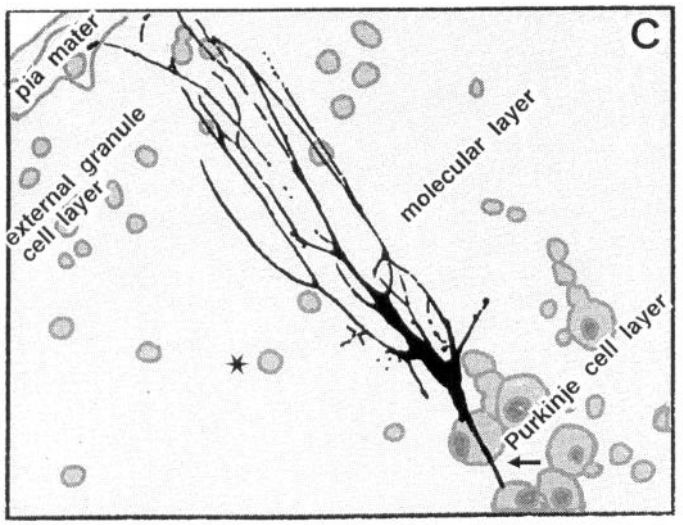

Figure 1. Bergmann glia in a cerebellar slice: topography and morphology at P6. *A*, A cerebellar slice from P6 is shown with differential interference contrast combined with fluorescence illumination to mark the position of a Lucifer yellow–stained Bergmann glia cell. A process of that Lucifer yellow–filled cell is indicated by the *arrow*. The *asterisk* marks a granule cell migrating through the molecular layer. *B*, In the same field as shown in *A*, the Lucifer yellow–filled Bergmann glial cell is shown with the fluorescence optics. *C*, A scheme of the cerebellar slice as shown in *A* was superimposed by a computer-based reconstruction of the Bergmann glia cell as derived from a series of photographs at different focal planes (one of these photographs is shown in *B*). The cerebellar layers are indicated. Scale bar, 50 μm.

those from P20–P30 slices, extended processes into the granule cell layer and, in some instances, along the Purkinje cell layer.

We have demonstrated previously that P20–P30 Bergmann glial cells injected with Lucifer yellow are immunoreactive for GFAP, which identifies them as astrocyte-like cells (Müller et al., 1992).

Bergmann glial cells resting membrane potential

The resting membrane potential of Bergmann glial cells was determined briefly after establishing the whole-cell recording configuration. No variation was observed among cells from animals of different ages, since it averaged −64 mV (range, −50 to −78 mV; $N = 20$) for cells from P5–P7 slices, −67 mV (range, −60 to −72 mV; $N = 20$) for cells from P10–P12 slices, and −68 mV (range, −56 to −80 mV; $N = 20$) for cells from P20–P30 slices.

Passive K^+ current in Bergmann glial cells

Membrane currents were recorded while stepping the membrane to a series of de- and hyperpolarizing potentials starting from −70 mV, using a voltage-clamp protocol. Small depolarizations (up to −30 mV) or hyperpolarizations (to −80 mV) induced a time-independent passive current ($N = 20$; Fig. 2) with a conductance of about 5 nS. This passive current was consistently observed in each age group.

As expected for a K^+-selective conductance, the reversal potential of the passive current followed the K^+ gradient: increasing the extracellular potassium concentration from 5 to 25 mM shifted the reversal potential from −80 to −40 mV, values in close agreement with those calculated with the Nernst equation for a K^+-selective conductance (−80 to −41 mV). In addition, the passive current increased in amplitude when the extracellular K^+ concentration was raised.

The passive current was only slightly affected by the various K^+ channel blockers, Ba^{2+} (71–84% of control value; $N = 5$; Fig. 3*D*), 4-AP (80 to 92% of control value; $N = 9$; Fig. 3*E*), and TEA (80–100% of control value; $N = 9$; Fig. 3*F*), as measured in cells from P20–P30 mice. In contrast, the passive current was markedly reduced when the cytosolic Ca^{2+} concentration was increased by addition of the Ca^{2+} ionophore ionomycin (29–82% of the control value within the first 3 min after application; $N = 8$). The ATP-sensitive K^+ channel activator pinacidil (10^{-4} M) and blocker gilbecamide (10^{-4} M) had no influence on the passive current.

Evidence for activation of voltage-gated currents in Bergmann glial cells from P5–P7 mice

Depolarization of P5–P7 Bergmann glial cells to potentials of −10 or −20 mV activated an outward current component that displayed a delayed increase during the voltage step. The time constant of activation averaged 76 msec (range, 27–157 msec; $N = 10$; Fig. 2*B*) for a voltage step from −70 to 20 mV. The conductance of this current component, calculated by subtracting the conductance of the passive current recorded at −50 mV,

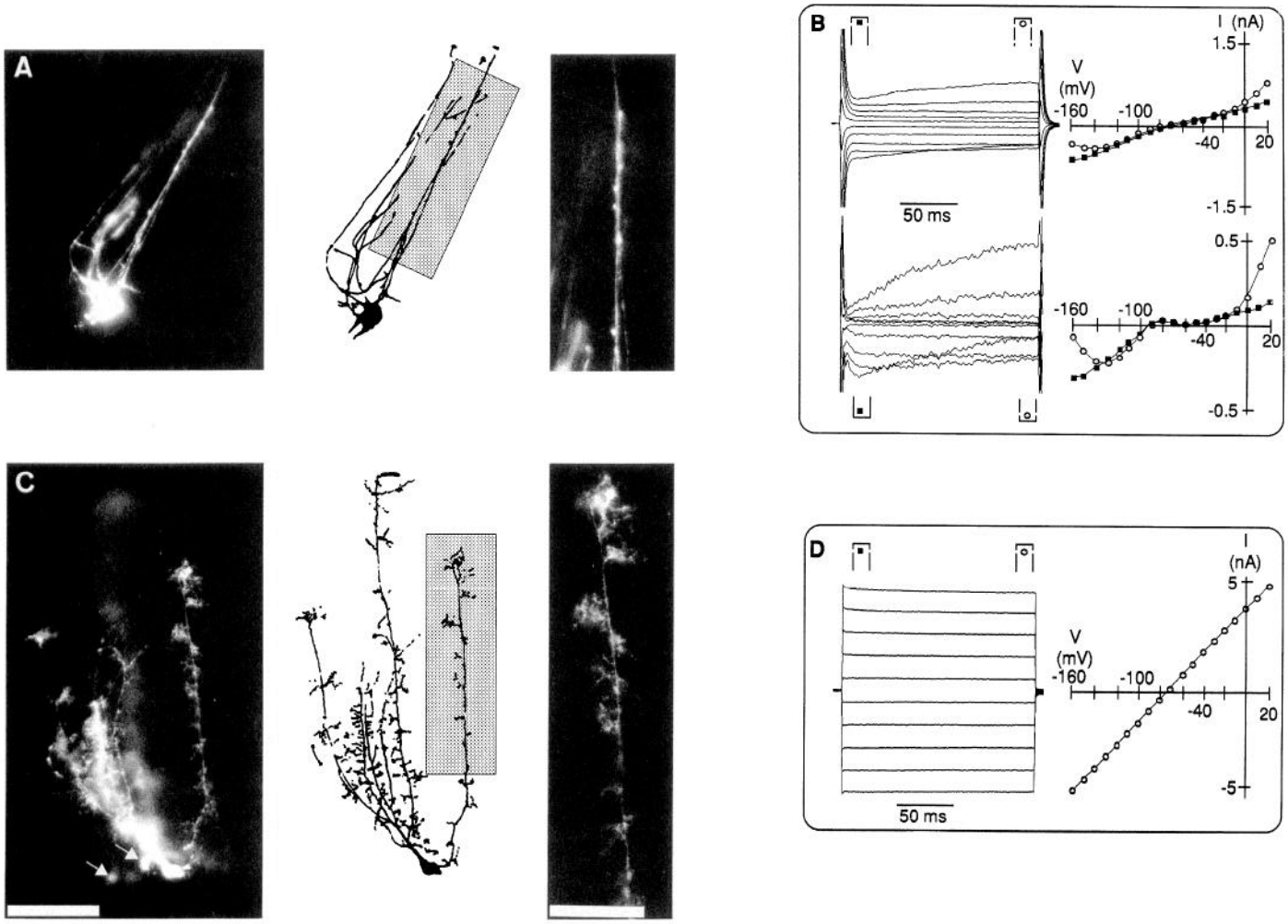

Figure 2. Bergmann glia in a cerebellar slice: morphological and electrophysiological features at different developmental stages. *A*, On the *left*, a Lucifer yellow–injected Bergmann glial cell from P6 is shown in the fluorescence micrograph. In the *middle*, the morphological features were reconstructed by computer based on a series of photographs taken at different focal planes. On the *right*, a process from that cell (see *box* in the *middle*) is shown at higher magnification. *B*, Using a voltage-clamp protocol, the membrane was clamped from a holding potential of −70 mV to increasing de- and hyperpolarizing potentials. The superimposed current responses to voltage jumps of −160, −140, −120, −100, −80, −60, −40, −20, 0, and +20 mV are shown. Young Bergmann glial cells (P6) responded to large de- and hyperpolarizations by activation of voltage-dependent currents. On the *right* the current (*I*)/voltage (*V*) curves were constructed from the currents on the *left*. The *squares* correspond to currents at the beginning (after 3 msec) of the voltage jump; the *circles*, to currents after the voltage jump. The *lower half* of *B* displays voltage-dependent currents from the cell shown in *upper half*, from which the passive currents activated by a voltage jump from −70 mV to −90 mV were subtracted. The *I/V* curves of the voltage-dependent currents shown on the right at the beginning (*squares*) and the end (*circles*) of the voltage jump are displayed (*right graph*). *C*, Similarly as described in *A*, a Bergmann glial cell from P20 is depicted. Note the numerous elaborated appendages on the processes of the P20 cell, as compared to the P6 cell. In the background a few weakly coupled cell bodies of adjacent Bergmann glial cells are visible (*arrows*). *D*, Using the same voltage-clamp protocol as in *B*, Bergmann glial cells from P20 responded to de- and hyperpolarizing voltages by large time- and voltage-independent currents. Scale bars in *C*: *left*, 50 μm; *right*, 25 μm.

amounted to about 4 nS ($N = 10$). In 4 of 20 cells, this delayed outward-rectifying current was not observed.

Hyperpolarization to potentials more negative than −80 mV activated an additional current component with an average conductance of 3 nS ($N = 10$). This inwardly rectifying current inactivated at potentials more negative than −140 mV. The time constant of inactivation decreased with hyperpolarization to reach 87 msec at −160 mV (range, 51–104 msec; $N = 20$; Fig. 2*B*). In three cells out of 20, no inward-rectifying current was observed, while two cells lacked both the inward-rectifying and the delayed outward-rectifying current.

These voltage-activated currents were not observed in cells from P20–P30 slices, and only in a fraction of cells in P10–P12 slices. In a sample of 20 cells in the latter age-group, four cells exhibited both the delayed outward-rectifying and inward-rectifying currents, and eight cells had only the inward-rectifying current component.

Ionic dependence of the voltage-gated currents

In cells from P5–P7 slices increasing the extracellular K^+ concentration from 5 to 55 mM caused a shift in reversal potential from −70 to −20 mV, corresponding to that predicted by the Nernst equation. In an elevated external K^+ concentration, the delayed outward-rectifier and inward-rectifier currents could no longer be observed (Sakmann and Trube, 1983).

The K^+ specificity of these currents was further characterized by testing the effects of K^+ channel blockers on the membrane conductance. Application of 5 mM Ba^{2+} or 10 mM 4-AP sig-

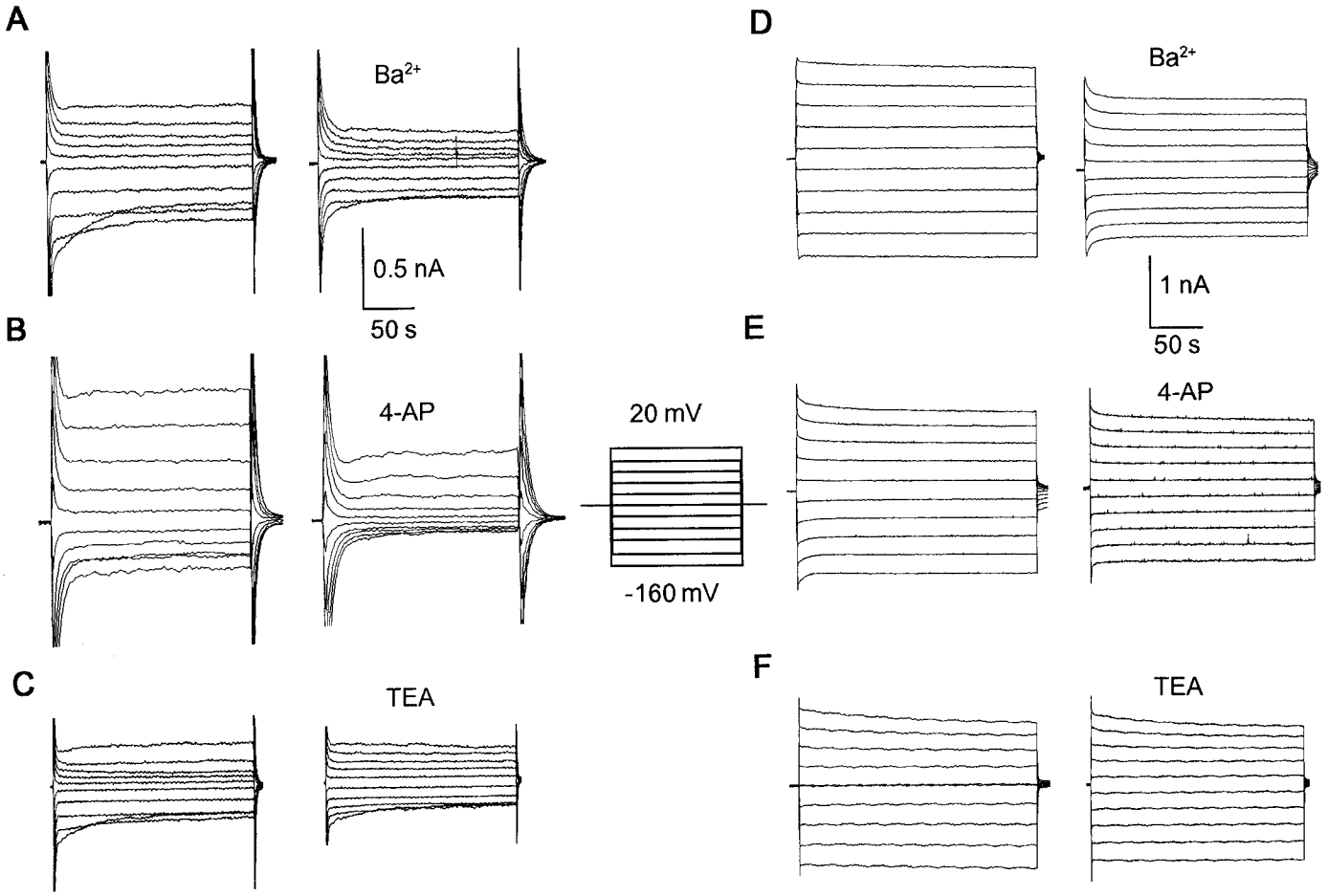

Figure 3. Effects of K^+-channel blockers on voltage-activated currents. Currents were activated as described for Figure 2. *A–C*, Recordings from a P6 cell. *D–F*, Recordings from a P20 cell. Application of 5 mM Ba^{2+} reduced both the inward- and outward-rectifying currents in young Bergmann glial cells (*A*). A similar effect was observed in presence of 10 mM 4-AP (*B*). In contrast, 50 mM TEA had a less pronounced effect on the inward-rectifying current, although clearly reducing the delayed outward current (*C*). In the P20 cell, Ba^{2+} was only slightly effective (*D*), and TEA and 4-AP had no effect (*E, F*).

nificantly reduced both the delayed outward-rectifier and the inward-rectifier currents (for Ba^{2+}: 9–35% of control value, $N = 7$; for 4-AP: 35–70% of control value, $N = 6$; see Fig. 3*A,B*). In contrast, 50 mM TEA, while clearly blocking the delayed outward-rectifier current (68–95%), had only a marginal effect on the inward-rectifier current ($N = 7$; Fig. 3*C*).

Effects of GABA on Bergmann glial cell membrane currents

The current evoked by application of 1 mM GABA to cells from P5–P7 slices had a mean peak amplitude of 901 pA (range, 362–1874 pA; $N = 19$; Fig. 4*A*) at the holding potential of −70 mV. This current typically activated within 5 sec and decayed to 50% of the peak value within 3 sec while GABA was still present in the bath. At lower concentrations (10^{-5} M, 10^{-4} M) GABA induced an inward current with a slower inactivation and a significant noise increase (see also Fig. 8*C*). In cells of P10–P12 mice the GABA-mediated current showed a similar amplitude and time course as in younger ones (mean, 1360 pA; range, 416–2392 pA; $N = 16$; Fig. 4*B*). In contrast, application of GABA produced only a weak inward current in the majority of Bergmann glial cells obtained from P20–P30 animals (24 of 29 cells; mean, 111 pA; range, 10–440 pA; $N = 24$, Fig. 4*C*) and in the remaining five cells (17% of the sample) the current response was below noise level (5 pA).

Reversal potential and ionic dependence of GABA-activated currents

To identify the ionic species mediating the current activated by GABA, we mainly used cells from P5 to P12, since large GABA responses were activated and thus are better analyzed. The reversal potential of the GABA response was determined while K^+ currents were blocked by preincubation of the slices with Ba^{2+} for 10 min. GABA was applied in the presence of Ba^{2+} and the membrane was depolarized or hyperpolarized for 100 msec intervals to −40, −20, 0, +20, +40, +60, +100, and −105 mV to establish current/voltage relationships at 2 sec intervals. The current induced by GABA was obtained by subtracting the current measured before the application of GABA from that observed at the peak of the GABA response (Fig. 5). The average reversal potential was approximately +10 mV (range, 0 to +20 mV; $N = 10$; Fig. 5*A*), indicating that GABA activated mainly a chloride conductance ($E_{Cl^-} = -5$ mV for the Cl^- concentration in the pipette and in the bath solution). The average conductance increase induced by GABA was 10 nS.

To elucidate the ionic composition of the GABA current, we replaced 150 mM external sodium chloride by 150 mM choline chloride or 150 mM sodium gluconate. While the substitution of sodium by choline had no effect on the reversal potential of

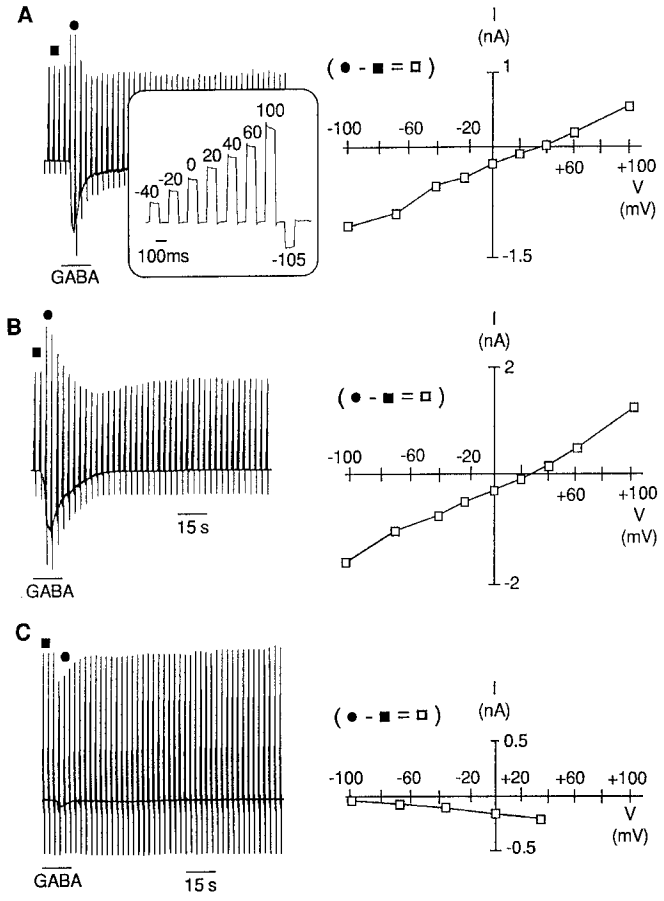

Figure 4. Age dependence of GABA-induced currents. Cells were recorded from slices obtained from animals at P6 (*A*), P10 (*B*), and P20 (*C*). Using a voltage-clamp protocol, the membrane was depolarized or hyperpolarized for 100 msec intervals from the holding potential at −70 mV to −40, −20, 0, +20, +40, +60, +100, and −105 mV (see *inset* in *A*) and the resulting current responses are displayed on the *left*. From these recordings, *I/V* curves were constructed at 2 sec intervals. The current corresponding to three sequences of voltage steps prior to application of GABA was averaged. These control currents (*solid squares*) were subtracted from currents at the peak of the GABA response (*circles*) to obtain the *I/V* relationship of the GABA induced current (*open squares*) as shown on the *right*.

the GABA-induced current, the exchange of chloride by gluconate shifted the reversal potential to values beyond +100 mV. Although this value is much higher than the calculated Cl^- reversal potential of +70 mV by Nernst, this might be caused by an imperfect clamp control at these positive potentials as discussed below. However, both experiments suggest that Cl^-, but not Na^+, is the dominant charge carrier of the GABA-induced current in Bergmann glial cells.

In the absence of Ba^{2+}, Bergmann glial cells exhibited two types of responses to GABA. One population of cells (60%) was characterized by a biphasic response, namely, a GABA-induced conductance increase followed by a small conductance decrease (Fig. 6*A*). The reversal potential of the current activated by GABA was at +30 mV (range, +20 to +40 mV; $N = 10$), a value considerably higher than that measured in the presence of Ba^{2+}. The inward current recorded at −70 mV in the control solution was also 25% smaller than that recorded from the same cell in the presence of Ba^{2+} (Fig. 5). In the second phase, a 24% conductance decrease was observed, which lasted for about 1 min (range, 30 sec to 3 min). The reversal potential of the current inactivated by GABA was close to the equilibrium potential of K^+, namely, −85 mV (range, −75 to −105 mV; $N = 10$; Fig. 6*B*). In 40% of the Bergmann glial cells from P5–P12 slices, GABA induced only a decrease in membrane conductance (mean, 29%; range, 23–38%; $N = 8$; Fig. 6*B*), with a time course similar to that observed in the cells with the biphasic response. In both cases, this decrease was totally reversible. We thus conclude that GABA may exert a dual effect on Bergmann glial cells from P5–P12 slices: activation of a Cl^- conductance, best seen in the presence of Ba^{2+}, and reduction of the resting K^+ conductance.

In P20–P30 slices GABA had a much smaller influence on the membrane conductance of Bergmann glial cells. A small decrease was observed in the majority (69%) of cells (mean, 7%; range, 2–16%; $N = 12$). The reversal potential of this current was about −105 mV (Fig. 4*C*), close to the K^+ equilibrium potential. In the remaining cells, GABA induced a small increase in the membrane conductance (0–5%) with a reversal potential of about 100 mV (not shown).

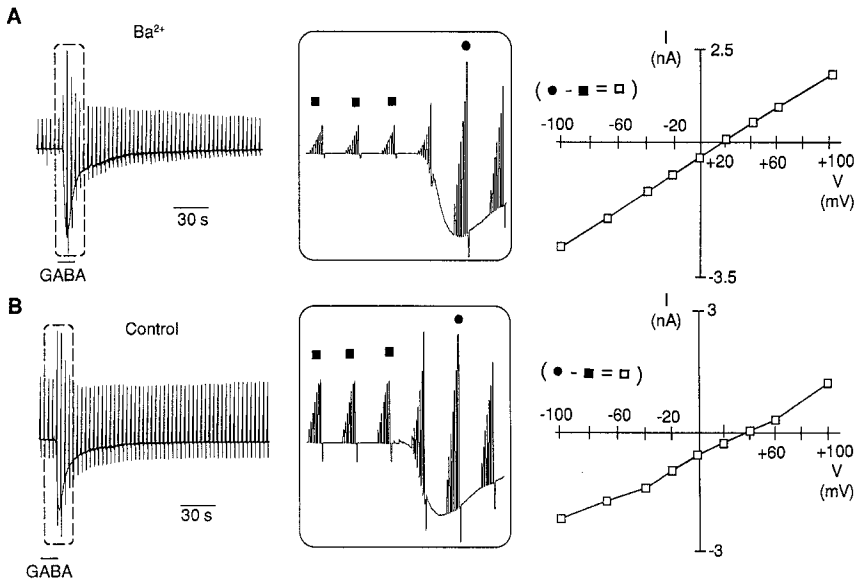

Figure 5. Current/voltage relationships of the GABA-induced currents: effect of Ba^{2+}. *A*, Membrane currents activated by application of 10^{-3} M GABA in a P6 Bergmann glial cell were analyzed while blocking part of the resting K^+ conductance. GABA was applied as indicated by the *bar* while the membrane was clamped to different potentials as described for Figure 4. The *inset* is an enlargement of the *boxed area* shown in the *left trace*. *I/V* curves are shown on the *right*. *B*, A similar protocol was performed on the same cell following replacement of the Ba^{2+}-containing solution with control solution. Note the shift of the reversal potential as compared to the response in the presence of Ba^{2+}.

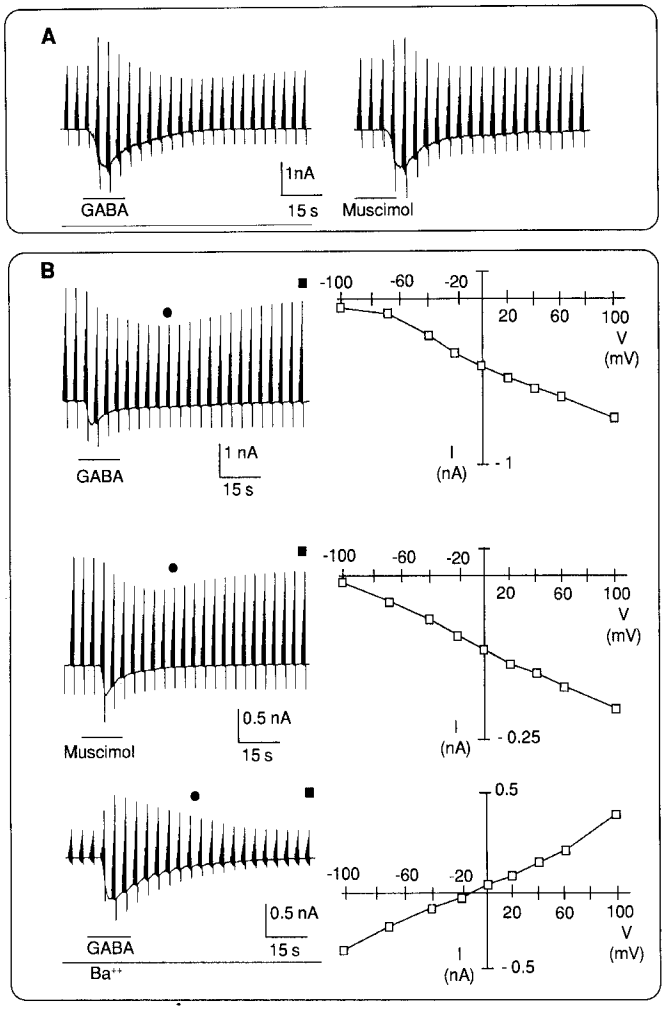

Figure 6. GABA- and muscimol-induced conductance decrease: effect of Ba^{2+}. *A*, Biphasic responses to GABA and muscimol in a P6 Bergmann glial cell. A series of voltage jumps was performed as described for Figure 4. GABA (10^{-3} M) and muscimol (10^{-3} M) were applied on the same cell, as indicated by the *bars*. *B*, GABA- and muscimol-induced decreases in membrane conductance in a P6 Bergmann glial cell were analyzed using the same procedure as in *A* (*upper* and *middle traces*). On the *right* the corresponding *I/V* curves of the current component blocked by GABA were determined by subtracting currents at the peak of the conductance decrease (*circle*) from those 120 sec after application of GABA (*solid squares*). Addition of Ba^{2+} (10 mM, *lower traces*) to the same cell induced a decrease in the resting membrane conductance, indicated by the smaller currents elicited by de- and hyperpolarizing voltage steps prior to application of GABA. Subsequently, GABA (10^{-3} M) was applied as indicated. The *I/V* curve obtained at similar time points as recordings in the absence of Ba^{2+} revealed clear conductance increase. The *I/V* curve of the GABA-induced currents shows a reversal potential at about 0 mV.

Pharmacological properties of the GABA-activated currents

The pharmacological properties of the currents induced by GABA were analyzed in cells that gave responses of large amplitudes, mostly from P5–P12 slices. A few cells from P20–P30 slices were also tested, which exhibited pharmacological properties similar to those seen in cells from younger animals.

The $GABA_A$ receptor agonist muscimol (10^{-4} M) mimicked the effects of GABA (10^{-4} M) by producing either a biphasic response with a conductance increase followed by a decrease (Fig. 6*A*) or a monophasic response with a conductance decrease only (Fig. 6*B*). In cells with a biphasic response the conductance decrease induced by muscimol was sometimes less apparent

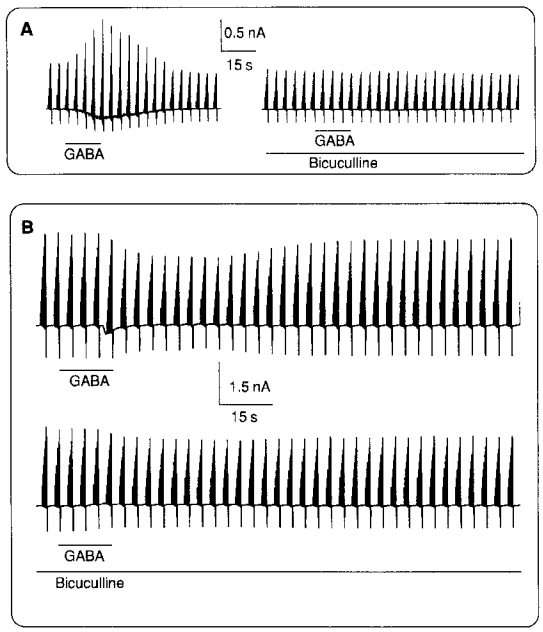

Figure 7. Effect of bicuculline on GABA responses. *A*, Membrane currents were activated as described for Figure 4 to record the GABA-induced currents in a P6 Bergmann glial cell. On the *left*, GABA (10^{-3} M) was applied in control solution; on the *right*, in the presence of bicuculline (10^{-4} M). The GABA-induced currents are blocked by bicuculline. *B*, With a similar protocol, currents were recorded from another Bergmann glial cell from P6, where GABA (10^{-3} M) caused a longer-lasting conductance decrease (control solution, *upper trace*). This conductance decrease as observed in the control solution is blocked in the presence of bicuculline (10^{-4} M; *lower trace*).

than with GABA (Fig. 6*A,B*). The mean peak amplitude of the current induced by muscimol in cells clamped at −70 mV was 101% of the peak response induced by GABA (83–111%, N = 5).

The competitive $GABA_A$ receptor antagonist bicuculline (10^{-4} M) was characterized following preincubation for 2 min and subsequent coapplication with 10^{-3} M GABA. The GABA-activated inward current was reduced in the presence of bicuculline to 17% of control levels (5–26%, N = 6; see Fig. 8*A*) when the membrane was clamped at −70 mV. Application of bicuculline alone did not affect the membrane currents. When the membrane conductance was analyzed using the voltage jump protocol as described above, both the increase in conductance and the following conductance decrease were abolished in the presence of bicuculline (Fig. 7*A,B*). Pentobarbital (10^{-4} M) potentiated the GABA-activated (10^{-4} M) current nearly twofold to a value of 181% of control (150–224%, N = 5; Fig. 8*A*). Diazepam (10^{-4} M), a benzodiazepine receptor agonist, and Ro-15-4513 (10^{-4} M), a benzodiazepine receptor inverse agonist, had no effects on GABA (10^{-5} M) responses (Fig. 8*B,C*).

Developmental maturation of $GABA_A$ receptor subunit immunoreactivities in Bergmann glial cells

Expression of $GABA_A$ receptors by Bergmann glial cells was monitored during postnatal development with subunit-specific antibodies against the α1-, α2-, α3-, β2,3-, and δ-subunits. In preliminary experiments, an antiserum against the γ2-subunit was also tested. In contrast to adult brain (Fritschy et al., 1992), this antiserum produced only a very light staining in the early developing brain and was therefore not suitable for the present study. For immunohistochemical experiments with the α1-, α2-,

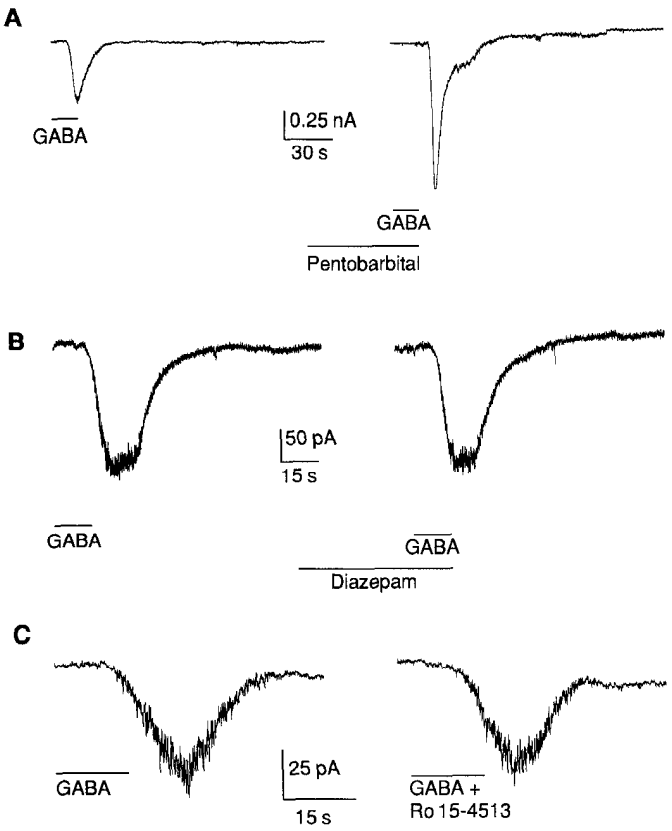

Figure 8. Pharmacological properties of the GABA response. *A*, Potentiation of the GABA response by pentobarbital. A 2 min preincubation with 10^{-4} M pentobarbital resulted in a clear increase of the GABA-induced (10^{-4} M) current at the holding potential of −70 mV. *B* and *C*, Lack of effects of the benzodiazepine agonist diazepam (5×10^{-4} M) and inverse agonist Ro-15-4513 (10^{-4} M) on GABA-induced (5×10^{-4} M) currents in a cell clamped at −70 mV. Notice the current noise increase during GABA application in *C*.

α3-, β2,3-, and δ-subunits, sections from rat brain were mainly used since these antibodies were raised against peptide sequences derived from rat cDNAs. Staining of mice brain sections was performed in a few cases, which revealed a staining pattern identical to that seen in the rat, although the staining intensity was generally lower.

In cerebellar sections, neurons were prominently stained and exhibited dramatic alterations during postnatal development (Figs. 7, 8). For instance, the α2-subunit transiently decorated the granule cells between P5 and P14, whereas the δ-subunit stained the Purkinje cells up to P10–P14, but not thereafter. The staining pattern of the α2- and δ-subunits is illustrated in Figure 9. A detailed account of the postnatal maturation of $GABA_A$ receptor expression in cerebellar neurons will be given elsewhere (G. D. Pratt, J.M. Fritschy, and H. Möller, unpublished observations). In addition, Bergmann glial cells were distinctly stained with the α2-, α3-, and δ-subunits antibodies (Fig. 9). With each of these three antibodies, staining of the Bergmann glial cells was first seen around P5, became most prominent at P7–P10, and decreased gradually thereafter. At P20, staining of the Bergmann glial cells had virtually disappeared, except for a faint α2-subunit immunoreactivity (Fig. 9). As compared to neurons, the staining intensity of Bergmann glial cells was relatively weak. While the large processes radially spanning the molecular and external granule layer were distinctly visible, the fine processes and end-feet revealed by the intracellular injections of Lucifer yellow (see above) could not be detected. The α1-subunit antiserum and the monoclonal antibody bd-17, which produced an intense staining of both the Purkinje and granule cells, failed to decorate the Bergmann glial cells at any of the time points examined (Fig. 10).

Double-immunofluorescence experiments in P10 rat sections showed that staining for GFAP is colocalized with staining for the $GABA_A$ receptor subunits α2, α3, and δ within individual Bergmann glial cell bodies and processes. At high magnification, double staining was evident within fine processes and local appendages. Moreover, staining for the $GABA_A$ receptor subunits appeared punctate, in particular for the α2-subunit (Fig. 11), suggesting local aggregations of receptor subunits along the Bergmann glial cell processes.

Discussion

Maturation of the membrane properties of Bergmann glial cells

The present results demonstrate that the membrane properties of Bergmann glial cells change during maturation of the cerebellum. While cells at each age exhibit prominent K^+ currents, two principal differences were observed between cells from P5–P7 and cells from P20–P30 mice. (1) Young Bergmann glial cells exhibit voltage-dependent currents, mediated by a delayed-rectifier and an inward-rectifier K^+ channel. While the inward rectifier resembles those of other glial cells (Barres et al., 1990), the delayed outward rectifier differs by a more positive threshold potential (Sontheimer et al., 1989). At P20–P30, only passive K^+ conductances were observed. (2) Application of GABA to young Bergmann glial cells activates a pronounced membrane current, whereas GABA has only minor effects on most Bergmann glial cells from older mice.

The variability in the occurrence of voltage-activated currents amongst cells from one age group may reflect a heterogeneity in developmental stages of individual Bergmann glial cells. We also cannot exclude that this differences may be caused by variabilities in the voltage-clamp control.

Transient expression of $GABA_A$ receptors by young Bergmann glial cells: electrophysiological evidence

The majority of cells responding to GABA exhibit a biphasic response dominated by a conductance increase. In the remaining

→

Figure 9. Developmental changes in α2- and δ-subunit immunoreactivities in the cerebellum: photomicrographs depicting the transient α2- and δ-subunit immunoreactivity in rat Bergmann glial cells at P10 and P20, visualized by immunoperoxidase staining. A 2.5× enlargement of the framed area is shown in the *middle row*. At P10, notice the staining of Bergmann glial cell somata (*arrows*) and radial processes (*arrowheads*), which span the molecular layer (*ML*) and the external granule layer (*EGL*). In addition to Bergmann glial cells, the α2-subunit antibody decorated the granule cells in the internal granule cell layer (*IGL*) and the δ-subunit antibody stained Purkinje cells. At P20, α2-subunit staining was markedly decreased in Bergmann glial cells (*arrowheads*) and granule cells, but Golgi type II cells (*arrow*) were distinctly stained; at this time point, δ-subunit staining had disappeared from Bergmann glial cells and Purkinje cells, but was very intense in the internal granule cell layer. Parasagittal sections through the vermis photographed with differential interference contrast filters. Scale bars, 50 μm.

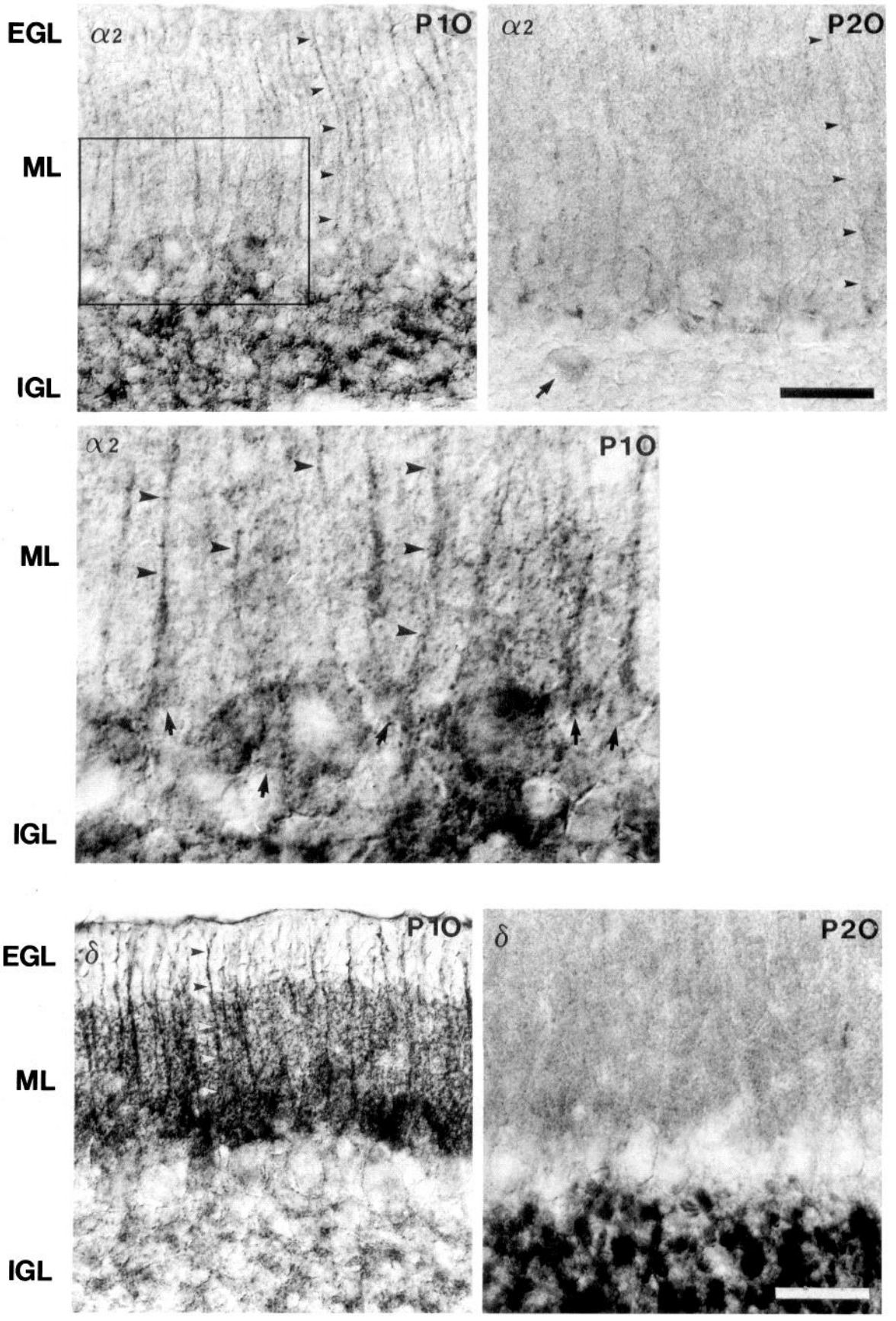
EGL
ML
IGL
α2
P10
α2
P20
α2
P10
ML
IGL
EGL
δ
P10
δ
P20
ML
IGL

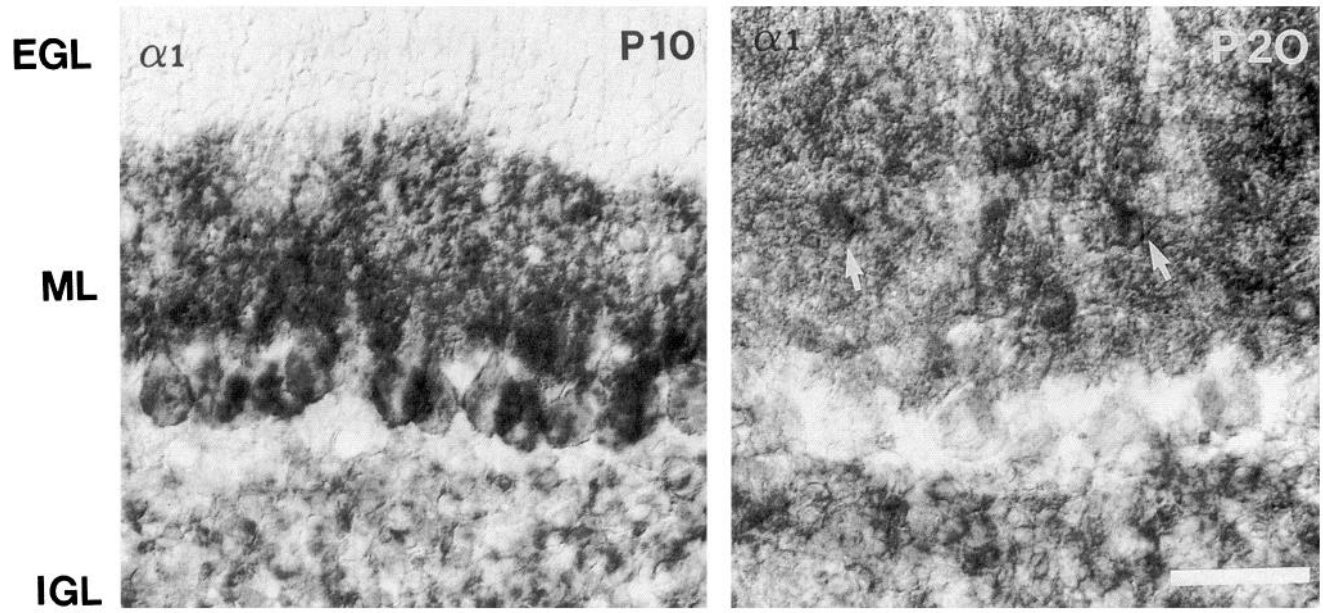

Figure 10. Lack of α1-subunit staining in Bergmann glial cells: immunoperoxidase staining of cerebellar sections with the α1-subunit antiserum at P10 and P20, showing the lack of Bergmann glial cell staining with this antibody, in contrast to the intense neuronal staining. At P10, Purkinje cell bodies and dendrites were intensely stained, as well as the granule cells. At P20, staining of Purkinje cell dendrites was reduced, and interneurons in the molecular layer became apparent (*arrow*). Scale bar, 20 μm.

cells, only a delayed conductance decrease was observed. The pharmacological profile of the current activated by GABA indicates that it is mediated via GABA$_A$ receptors. Indeed, both effects of GABA, the conductance increase and the decrease, can be mimicked by the specific GABA$_A$ receptor agonist muscimol (Fig. 6) and blocked by the antagonist bicuculline (Fig. 7). The barbiturate pentobarbital enhanced the GABA activated inward current. In the presence of Ba^{2+}, the reversal potential of the GABA-activated current was close to +10 mV, a value compatible with the equilibrium potential predicted for the Cl^- channel contained within the GABA$_A$ receptor (Bormann and Kettenmann, 1988). Moreover, a current noise increase was seen during GABA application, which points to the activation of ion channels by GABA. Similar GABA-activated currents have been reported in other glial cells (von Blankenfeld and Kettenmann, 1992) and in neurons (Bormann, 1988). However, the GABA$_A$ receptor present in Bergmann glial cells is unique in that it is insensitive to benzodiazepine-receptor agonists and inverse agonists.

The delayed conductance decrease induced by GABA is characterized by a reversal potential close to the K^+ equilibrium potential. Since this effect of GABA was mimicked by muscimol and blocked by bicuculline, we conclude that like the Cl^--mediated conductance increase, it is mediated by GABA$_A$ receptors. However, the link between GABA$_A$ receptor activation and the decrease in the resting K^+ conductance remains to be investigated. The involvement of Ca^{2+} ions seems likely since the resting K^+ conductance is blocked by an increase in cytosolic Ca^{2+} (Müller et al., 1992). It is of note that activation of kainate receptors, which is also known to increase intracellular Ca^{2+} concentrations in Bergmann glial cells (Müller et al., 1992), leads to a similar transient blockade of the resting K^+ conductance.

Distribution of ion channels

Our electrophysiological data suggest that GABA$_A$ receptors in young Bergmann glial cells are predominantly located on the processes rather than on the cell body. The GABA-activated Cl^- channel was under imperfect voltage-clamp control in the normal bathing solution, since the reversal potential of the GABA-induced current was closer to the Cl^- equilibrium potential when K^+ channels were blocked by Ba^{2+}. This imperfect voltage-clamp control points to a predominant localization of GABA$_A$ receptors distant from the electrode, that is, on the processes of the Bergmann glial cells. A similar polarization of the distribution of the voltage-gated channels also seems likely. The activation threshold of the delayed-rectifying K^+ channel is more positive than in other glial cells, which suggests that this channel was not under good voltage-clamp control. This would imply that the majority of the channels are not on the soma, but rather on the processes.

Transient expression of GABA$_A$ receptor subunit immunoreactivity in Bergmann glial cells

Expression of GABA$_A$ receptors in Bergmann glial cells is under developmental control. This conclusion is based on our immunohistochemical findings that reveal a transient expression of the GABA$_A$ receptor α2-, α3-, and δ-subunits in Bergmann glial cells, with a time course similar to that revealed by the degree of electrophysiological responsiveness of the cells to GABA. Large GABA currents reflecting the activation of many receptors were seen almost exclusively in cells from P5–P12 animals. At P20, when the GABA responsiveness is almost absent, only the α2-subunit immunoreactivity was still detectable. A low level of expression of the α2-subunit is in agreement with the observations of Laurie et al. (1992) and Wisden et al. (1992) that adult Bergmann glial cells express the α2- and γ1-subunit mRNAs.

The γ2- and γ3-subunits have been reported to confer benzodiazepine sensitivity to recombinant receptors expressed in cell lines (Pritchett et al., 1989; Knoflach et al., 1991). Receptors containing the δ-subunit are thought to be insensitive to benzodiazepine-receptor ligands (Shivers et al., 1989), although re-

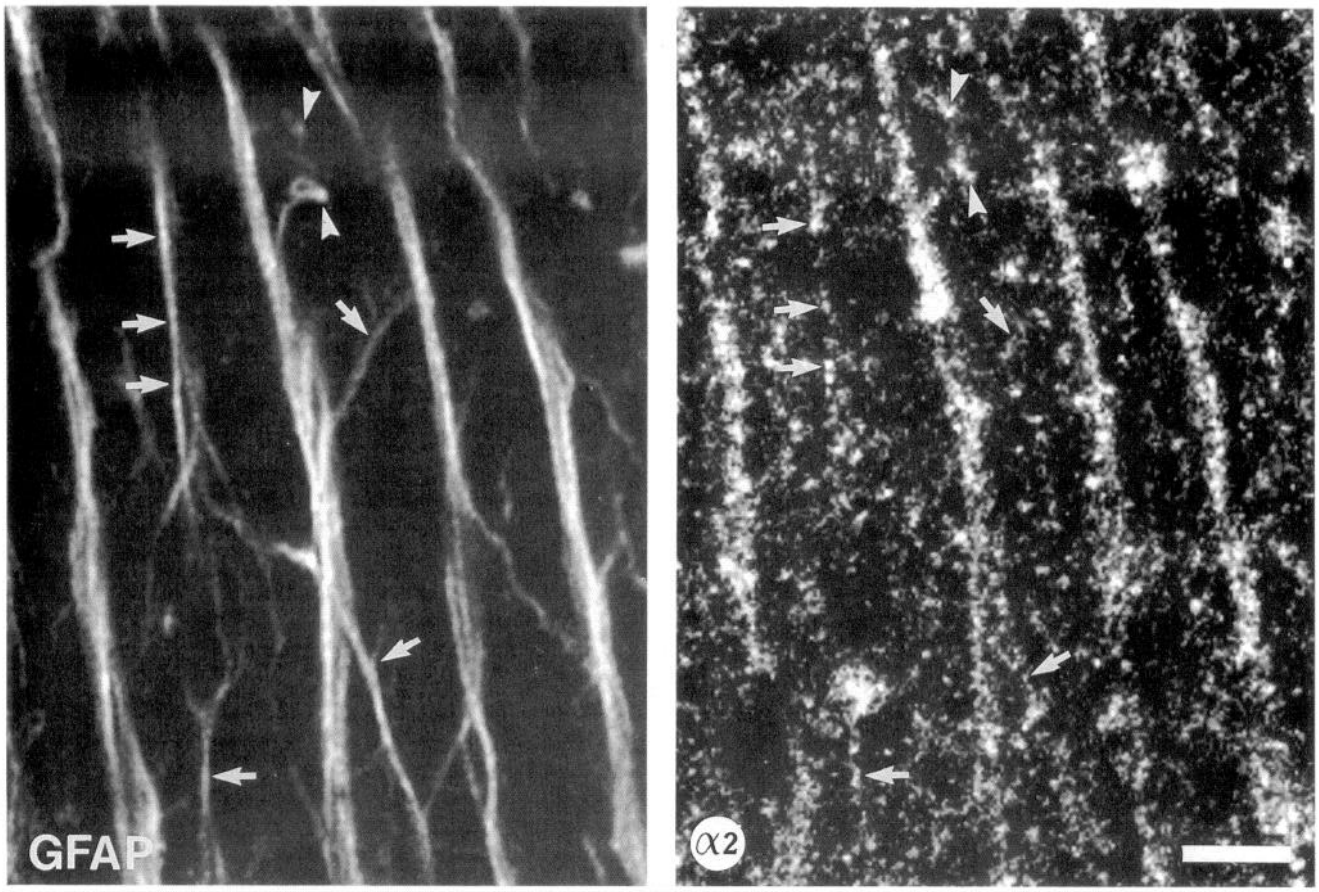

Figure 11. Colocalization of the α2-subunit with GFAP in Bergmann glial cell processes: video images from confocal laser microscopy displaying double-immunofluorescence staining of Bergmann glial cell processes with antibodies to GFAP (*left*) and to the $GABA_A$ receptor α2-subunit (*right*). Notice the punctate distribution of the α2-subunit immunoreactivity. *Arrowheads* point to α2-subunit–immunoreactive puncta localized in a GFAP-positive appendage that stems from a large process; *arrows* show α2-subunit staining in several fine processes immunoreactive for GFAP. Scale bar, 10 μm.

cent experiments show that at least some of the receptors with the δ-subunit also display a benzodiazepine binding site (Benke et al., 1991d). Elucidation of the full subunit composition of $GABA_A$ receptors expressed in Bergmann glial cells might therefore provide further clues about the structure of $GABA_A$ receptors lacking sensitivity to benzodiazepine receptor ligands.

Correlation between Bergmann glial cell function and the channel expression pattern

Expression of $GABA_A$ receptors and of voltage-gated channels in Bergmann glial cells is observed early during the development of the cerebellum, when these cells exhibit immature morphological features. In particular, young Bergmann glial cells lack the numerous appendages that characterize them at later stages of maturation. Since these cells serve as substrate for the migration of granule cells from the external granule layer to the internal granular layer, it is likely that this migratory process occurs before the appearance of these characteristic appendages.

The expression of GABA-activated and voltage-sensitive currents in Bergmann glial cells largely coincides with the period of migration of granule cells. Since GABA is thought to modulate maturation and differentiation of brain cells during development (Chronwall and Wolff, 1980; Lauder et al., 1986; see Meier et al., 1991, for review), several hypotheses may be formulated about the putative functional roles of these channels. First, it is possible that GABA modulates the maturation of Bergmann glial cells by means of $GABA_A$ receptors. Second, it is conceivable that activation of $GABA_A$ receptors influences the migration of granule cells. Third, since an upregulation in the expression of ionic currents was reported for astrocytes in contact with neurons (Barres et al., 1990), the presence of the granule cells on the Bergmann glial cell processes may influence the expression of these channels. With regard to the source of GABA in early development, cerebellar interneurons have been reported to be immunoreactive for GABA as early as P1 (basket cells) and P7 (stellate cells) (Aoki et al., 1989), while migrating granule cells do not express detectable levels of GABA. In conclusion, our results demonstrate the transient expression of ion- and voltage-gated channels on Bergmann glial cells during development. Thus, signal transduction mechanisms involving glial cells may regulate specific glial–neuronal interactions in the cerebellum.

References

Aoki E, Semba R, Kashiwamata S (1989) When does GABA-like immunoreactivity appear in the rat cerebellar GABAergic neurons? Brain Res 502:245–251.

Backus KH, Kettenmann H, Schachner M (1988) Effect of benzodiazepines and pentobarbital on the GABA-induced depolarization in cultured astrocytes. Glia 1:132–140.

Barres BA, Chun LYY, Corey DP (1990) Ion channels in vertebrate glia. Annu Rev Neurosci 13:441–474.

Benke D, Cicin-Sain A, Mertens S, Mohler H (1991a) Immunochemical identification of the α1- and α3-subunits of the $GABA_A$-receptor in rat brain. J Recept Res 11:407–424.

Benke D, Mertens S, Möhler H (1991b) Ubiquitous presence of $GABA_A$-receptors containing the α1-subunit in rat brain demonstrated by immunoprecipitation and immunohistochemistry. Mol Neuropharmacol 1:103–110.

Benke D, Mertens S, Trzeciak A, Gillessen D, Möhler H (1991c) $GABA_A$-receptors display association of γ2-subunit with α1- and β2/3 subunits. J Biol Chem 266:4478–4483.

Benke D, Mertens S, Trzeciak A, Gillessen D, Möhler H (1991d) Identification and immunohistochemical mapping of $GABA_A$-receptor subtypes containing the δ-subunit in rat brain. FEBS Lett 283:145–149.

Bormann J (1988) Electrophysiology of $GABA_A$ and $GABA_B$ receptor subtypes. Trends Neurosci 11:112–116.

Bormann J, Kettenmann H (1988) Patch clamp study of GABA receptor Cl^- channels in cultured astrocytes. Proc Natl Acad Sci USA 85:9336–9340.

Chronwall B, Wolff JR (1980) Prenatal and postnatal development of GABA-accumulating cells in the occipital neocortex of rat. J Comp Neurol 190:187–208.

Dodt HU, Zieglgänsberger W (1990) Visualizing unstained neurons in living brain slices by infrared DIC-videomicroscopy. Brain Res 537:333–336.

Edwards FA, Konnerth A, Sakmann B, Takahashi T (1989) A thin slice preparation for patch clamp recordings from neurones of the mammalian central nervous system. Pfluegers Arch 414:600–612.

Ewert M, Shivers BD, Luddens H, Möhler H, Seeburg PH (1990) Subunit selectivity and epitope characterization of mAbs directed against the $GABA_A$/benzodiazepine receptor. J Cell Biol 110:2043–2048.

Fritschy JM, Benke D, Mertens S, Oertel WH, Bachi T, Mohler H (1992) Five subtypes of type A gamma-aminobutyric acid receptors identified in neurons by double and triple immunofluorescence staining with subunit-specific antibodies. Proc Natl Acad Sci USA 89: 6726–6730.

Hamill OP, Marty A, Neher E, Sakmann B, Sigworth FJ (1981) Improved patch-clamp techniques for high-resolution current recording from cells and cell-free membrane patches. Pfluegers Arch 391:85–100.

Haring P, Stahli C, Schoch P, Takacs B, Staehelin T, Mohler H (1985) Monoclonal antibodies reveal structural homogeneity of γ-aminobutyric acid/benzodiazepine receptors in different brain areas. Proc Natl Acad Sci USA 82:4837–4841.

Hatten ME, Fishell G, Stitt TN, Mason CA (1990) Astroglia as a scaffold for development of the CNS. Semen Neurosci 2:455–465.

Hsu SM, Raine L, Fanger H (1981) Use of avidin-biotin-peroxidase complex (ABC) in immunoperoxidase techniques: a comparison between ABC and unlabeled antibody (PAP) procedures. J Histochem Cytochem 29:577–580

Ito M (1984) The cerebellum and neural control. New York: Raven.

Knoflach F, Rhyner T, Villa M, Kellenberger S, Drescher U, Malherbe P, Sigel E, Mohler H (1991) The γ3-subunit of the $GABA_A$-receptor confers sensitivity to benzodiazepine receptor ligands. FEBS Lett 293: 191–194.

Lauder JM, Han VKM, Henderson P, Verdoorn T, Towle AC (1986) Prenatal ontogeny of the GABAergic system in the rat brain: an immunocytochemical study. Neuroscience 19:465–493.

Laurie DJ, Seeburg PH, Wisden W (1992) The distribution of 13 $GABA_A$ receptor subunit mRNAs in the rat brain. II. Olfactory bulb and cerebellum. J Neurosci 12:1063–1076.

Marksitzer R, Benke D, Fritschy JM, Trzeciak A, Bannwarth W, Mohler H (1992) $GABA_A$-receptors: drug binding profile and distribution of receptors containing the α2-subunit *in situ*. J Recept Res 13:467–477.

Meier E, Hertz L, Schousboe A (1991) Neurotransmitters as developmental signals. Neurochem Int 19:1–15.

Müller T, Möller T, Berger T, Schnitzer J, Kettenmann H (1992) Calcium entry through kainate receptors and resulting potassium-channel blockade in Bergmann glial cells. Science 256:1563–1566.

Pritchett DB, Sontheimer H, Shivers BD, Ymer S, Kettenmann H, Schofield PR, Seeburg PH (1989) Importance of a novel $GABA_A$ receptor subunit for benzodiazepine pharmacology. Nature 338:582–585.

Rakic P (1981) Neuronal-glial interaction during brain development. Trends Neurosci 7:184–187.

Ramon y Cajal S (1909–1911) Reprinted in: Cerebellar cortex, p 291. Berlin: Springer, 1974.

Sakmann B, Trube G (1983) Voltage-dependent inactivation of inwardly rectifying single channel currents in guinea-pig heart cell membrane. J Physiol (Lond) 347:659–683.

Shivers BD, Killisch I, Sprengel R, Sontheimer H, Köhler M, Schofield PR, Seeburg PH (1989) Two novel $GABA_A$ receptor subunits exist in distinct neuronal subpopulations. Neuron 3:327–337.

Sontheimer H, Trotter J, Schachner M, Kettenmann H (1989) Channel expression correlates with differentiation stage during the development of oligodendrocytes from their precursor cells in culture. Neuron 2:1135–1145.

von Blankenfeld G, Kettenmann H (1992) Glutamate and GABA receptors in vertebrate glial cells. Mol Neurobiol 5:31–41.

Wisden W, Laurie DJ, Monyer H, Seeburg PH (1992) The distribution of 13 $GABA_A$ receptor subunit mRNAs in the rat brain. I. Telencephalon, mesencephalon. J Neurosci 12:1040–1062.